

**GT2021-59487**

## A NOVEL ENERGY STORAGE SYSTEM BASED ON CARBON DIOXIDE UNIQUE THERMODYNAMIC PROPERTIES

**Marco Astolfi**  
 Politecnico di Milano  
 Milano, Italy

**Dario Rizzi**  
 Energy Dome SpA  
 Lonate Pozzolo, Italy

**Ennio Macchi**  
 Politecnico di Milano  
 Milano, Italy

**Claudio Spadacini**  
 Energy Dome SpA  
 Lonate Pozzolo, Italy

### ABSTRACT

*This paper focuses on the thermodynamic performance and techno-economic assessment of a novel electrical energy storage technology using carbon dioxide as working fluid. This technology, named CO<sub>2</sub> battery and recently patented by Energy Dome SpA., addresses to an energy market which has great need of energy storage solutions able to handle the increasing share of non-dispatchable renewable energy sources like photovoltaic and wind energy. After a brief introduction, the present study presents the concept of CO<sub>2</sub> batteries and their operation. Then the detailed numerical model developed for the accurate calculation of system round trip efficiency is presented with the adopted assumptions and the optimization routine description. Results on the reference case and following sensitivity analysis confirm a RTE of around 77% ( $\pm 2\%$ ) which makes CO<sub>2</sub> batteries a very promising technology with respect to other energy storage systems based on thermodynamic cycles like compressed air and liquid air energy storage thanks to the high performance and the easiness of installation. Finally, calculation of system footprint, capital investment cost and levelized cost of storage are discussed.*

Keywords: Energy storage, CO<sub>2</sub> battery, carbon dioxide, round trip efficiency, economic assessment

### 1. INTRODUCTION

The common goal of progressively decarbonize the power production sector will result in next years in a strong increase of renewable energy contribution in the energy market. The most competitive renewable energy technologies are today solar PV and on shore wind turbines [1]. Their installed capacity has been increased dramatically in the last 5-10 years worldwide: +23.8% and +12.60% growth for solar and wind respectively in 2019 due to their significant cost decrease as well as to the availability of relevant economic incentives [2]. However, the main drawback of these renewable energy technologies is represented by the non-perfect forecasting and the intrinsic non-dispatchability that already today involves issues on the transmission grids

### NOMENCLATURE

BOP	Balance of Plant
CAES	Compressed Air Energy Storage
CCF	Carrying Charge Fraction
FP	Footprint
HRU	Heat Rejection Unit
HTF	Heat Transfer Fluid
HX	Heat Exchanger
$k_{is}$	stage load coefficient
LAES	Liquid Air Energy Storage
LCOS	Levelized Cost Of Storage
PCHX	Post Cooler Heat Exchanger
PHES	Pumped Hydro Energy Storage
PTES	Pumped Thermal Electricity Storage
Q	Thermal power
RTE	Round Trip Efficiency
T,p,h,s	temperature, pressure, specific enthalpy and specific entropy
TES	Thermal Energy Storage
$u_m$	mean diameter peripheral speed
W	electrical or mechanical power

management and requires a substantial transformation of the existing network [3]. The need of an affordable, efficient and sustainable energy storage technology is mandatory for the next generation energy market in order to allow large share of renewable energy but also ensure grid stability. Unfortunately, energy storage technologies available today lack in meeting these ambitious targets. Pumped hydro energy storage (PHES) is already mostly exploited and the possibility of new installations is strongly related to the availability of a proper site location orography. Electrochemical batteries are available in several different models, but all of them are far for offering a suitable solution for utility scale, long term energy storage. Lithium-ion technology is nowadays the most used thanks to its very high nominal round trip efficiency (RTE) around 95% [4]. However,

realistic RTE obtained considering real operation and accounting for all the auxiliary consumptions plus performance decay due to wearing and ageing, is lower than the nominal value and between 70% and 80% [5]. Finally, they are characterized by short lifetime 7-10 year when used with reduced depth of discharge [6], relevant replacement cost and issues related to disposal of equipment.

Compressed Air Energy Storage (CAES) can reach competitive RTE (around 70%-82% [7]) but it requires the availability of large underground caves [8] or deep seabed [9] and so it cannot freely located close to renewable energy production sites. Only few diabatic CAES systems have been installed and operated in different relevant size projects: examples are the 290 MW Huntorf plant (1978) and the 110 MW McIntosh plant (1991) [10] with efficiency of around 42% while adiabatic CAES as that studied in the 260 MW Adele project should reach efficiency around 70% [11].

Liquefied Air Energy Storage (LAES) is a promising solution that can limit the system footprint; however maximum RTE is expected to be in the range of 50%-60% [12] and it requires cryogenic air liquefaction equipment. Highview power [13] company is focused on the development of LAES technology and carried out experimental test on a cryogenic energy storage pilot plant (350kW/2.5MWh) between 2011 and 2014 and is operating the first grid scale (5MW/15MWh) demonstrator plant at Pilsworth Landfill facility in Bury, Greater Manchester from April 2018.

Green hydrogen storage shows lower RTE than other storage technologies with values between 35%-55%. This figure is due to the limited hydrogen production efficiency in the range of 65% (alkaline and PEM electrolyzers) and 90% (high temperature electrolyzers) and the limited discharge efficiency equal to 50%-60% (combined cycle power plants) [14]. Moreover, it entails safety issues related long term storage of a high flammability fluid.

Finally, pumped thermal electrical storage (PTES) are based on the use of electricity in charging mode to power an heat pump to transfer heat from a low temperature storage up to a high temperature storage and reversing the system operation in discharging mode. Usually PTES is proposed adopting closed Brayton cycles [15] and HP/ORC systems [16]. In this last case, if waste heat at middle temperature is available during charging mode the RTE can range between 50% and 100%, while on the contrary if both HP and ORC works with the same low temperature sink the maximum efficiency is around 30%. PTES is still far from penetration in the market although a pilot plant (150kW-600kWh) has been designed by Newcastle University and installed at Sir Joseph Swan Centre for Energy Research [17] and Malta Inc. is commercially proposing the technology [18]. Use of carbon dioxide has been proposed for different type of energy storage systems in place of air or organic fluids in order to increase the system round trip efficiency and to increase the energy density by reducing the footprint.

Carbon dioxide can be used in a CAES-like system exploiting two saline aquifers at different depths as storage reservoirs [19]. Transcritical (minimum storage pressure equal to 20 bar) and

supercritical (minimum storage pressure equal to 80 bar) configurations are investigated while maximum storage pressure is equal to 400 bar in both schemes. Different configurations are analyzed considering a different arrangement of multi-stage intercooled compressor and by adopting an additional natural gas heater to boost the cycle efficiency by increasing turbine inlet temperature up to 500°C in discharging phase. Thermal energy storage can be used to store compression heat during charging phase and exploit it during discharge phase but authors also discuss the possibility to avoid this component by exploiting the natural geothermal temperature gradient of the saline-aquifer reservoir. RTE is calculated dividing turbine power output by the sum of compressor consumption and the equivalent electricity attainable by the use of natural gas in a conventional power plant: calculated values are 63.35% for the transcritical cycle and 62.28% for the supercritical cycle. Energy density is around one order of magnitude higher than CAES solutions but main drawbacks are related to the very specific site location requirements with reservoirs at different depths (200-760 m for low pressure storage and 3000 m for the high pressure storage) and the use of fixed volume storage which implies a non-constant pressure ratio of turbomachinery during charging and discharging operations.

Carbon dioxide is also proposed as working medium in pumped thermal energy storage systems using both transcritical [20] and supercritical cycles [21]. Calculated RTE are between 42.5% and 55% for the transcritical cycle and can reach values around 70% in solar energy supported supercritical cycles.

In this scenario EnergyDome SpA [22] has patented an novel energy storage technology, called CO<sub>2</sub> battery, that aims to meet market requirements of affordability, efficiency and sustainability. This non-conventional energy storage solution is based on the close looping of CO<sub>2</sub> between gaseous form at ambient pressure and high pressure liquid status leading to a system that can benefit by high energy density but without the need of excessive pressures. This paper is focused on the numerical techno-economic assessment of CO<sub>2</sub> battery technology: first the system description is briefly introduced, then the numerical model, the assumptions and the optimization procedure are presented. Then, thermodynamic results and attainable performance are discussed with a comparison with other energy storage technologies. Finally, system footprint is calculated and cost analysis is proposed.

## 2. CO<sub>2</sub> BATTERY DESCRIPTION

Any electric storage system is made of two phases: a “charging phase”, whereby electric energy is used to store energy in some form (electrochemical, mechanical, thermal, gravitational, etc.) and a “discharging phase”, whereby the stored energy is used to produce electric energy. The present system uses electricity to compress a fluid (CO<sub>2</sub>) and its expansion to produce electricity. The following figure 1 illustrates the simplified layout of CO<sub>2</sub> battery and helps illustrating the basic idea of the proposed system.

The “charging” phase can be described by the following processes:

- The working fluid ( $\text{CO}_2$ ) is stored in the “dome” at ambient pressure and temperature and it enters the compressor (thermodynamic state #1);
- At the compressor exit (#2), the high pressure (70 bar), high temperature ( $450^\circ\text{C}$ ) fluid enters in the thermal storage system (TES), where is cooled down (#3) releasing thermal power to the heat carrier (not shown in the figure);
- The cooled  $\text{CO}_2$  (#3) enters a water-cooled condenser where it is condensed at 65.1 bar and possibly subcooled (#4). The cooling water flows in a closed loop with a large basin which work as a pseudo-recuperator between charging and discharging process. The liquid  $\text{CO}_2$  (#4) is stored in a series of pressure vessels.

The two net results of the charging phase are: (i) the storage of a relevant mass of liquid  $\text{CO}_2$  at high pressure and ambient temperature and (ii) the accumulation of a relevant amount of high temperature heat in the TES. This is obtained at the expense of the electrical energy required to compress the  $\text{CO}_2$  and to the circulation pumps of the heat carrier fluid and of the cooling water.

The “discharging” phase can be described by the following processes:

- The liquid  $\text{CO}_2$  is first throttled in a valve to reach the pressure established by the evaporator (#4), where the fluid is evaporated at 57.2 bar and slightly superheated (#3) exploiting the heat stored in the low temperature water loop during charging phase;
- The gaseous, high pressure  $\text{CO}_2$  enters (#3) the heat storage system, where heats up to high temperature (#2), recovering almost all the heat stored in the charging phase;
- The high temperature ( $430^\circ\text{C}$ ), high pressure (54.2 bar)  $\text{CO}_2$  (#2) expands in the turbine down to close ambient pressure, producing electrical energy;
- After the expansion (#1), the low pressure  $\text{CO}_2$  is cooled down (#1') by a water-cooled post-cooler heat exchanger (PCHX) and enters the dome at nearly atmospheric temperature.

The net results of the discharging cycle are the production of electric energy and the re-establishment of initial conditions of the system: all  $\text{CO}_2$  in the dome at atmospheric pressure, “cold” heat storage tanks and water basin at initial temperature.

To respect the overall energy balance, since the electricity introduced in the system in the charging phase is larger than the electricity produced in the discharging phase, some thermal energy must be released to the ambient involving the need of air-cooled heat exchanger.

The peculiarities of the proposed solution are:

- the adoption of a working fluid which changes its thermodynamic state from vapor to liquid and vice versa at high pressure and at temperatures close to the ambient without the need of cryogenic conditions;
- the adoption of a variable volume dome made by a flexible membrane which maintains constant the thermodynamic

conditions of the working fluid in the gaseous phase during the charging and discharging phases by varying its volume.

Differently from systems using air (or other gases) as a working fluid, this system maintains the same thermodynamic conditions irrespectively of the charge status of the storage: the inlet conditions to the compressor are always the same, the compressor pressure ratio is set only by the condensation pressure which is kept constant by liquid storage solution, the temperatures at TES are always the same. For this reason, power and energy balances will give the same result, i.e. the round trip efficiency computed from “instantaneous” power balances of the two phases will be the same resulting from time averaged energy balances. In a way, if one considers the sequence of a charging and discharging phases, the plant can be seen as a closed power cycle, whereby no heat input is present and the difference between the electric power introduced in the charging phase and produced in the discharging phase equals the thermal power released to the ambient.

### 3. NUMERICAL MODEL AND ASSUMPTION

In order to simulate the system performance, a numerical tool is implemented based on the plant layout reported in Figure 2. Carbon dioxide thermodynamic properties are calculated with REFPROP 9.1 [23] in order to catch the impact of real gas effects close to the saturation dome with high accuracy.

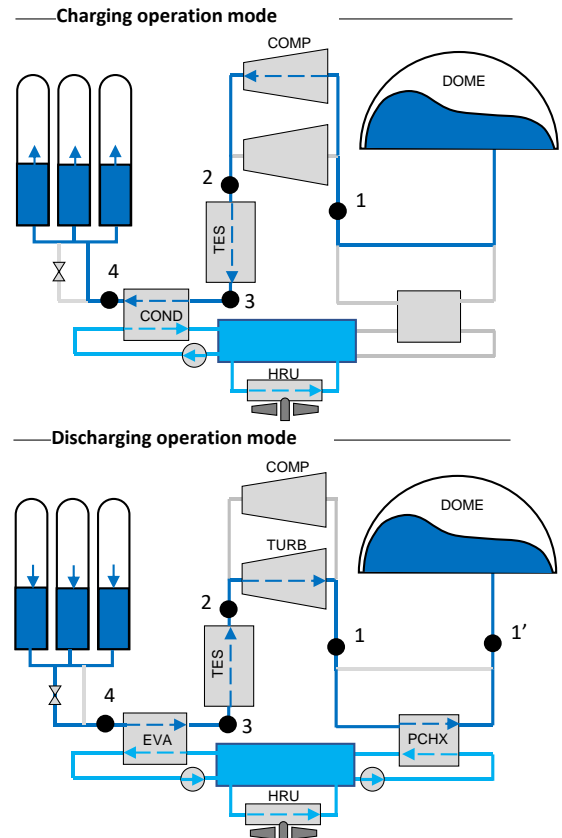


**FIGURE 1 – SIMPLIFIED  $\text{CO}_2$  BATTERY SCHEME IN CHARGING AND DISCHARGING MODES**

It can be noticed that the plant scheme is much more complex than the simplified one represented in Figure 1, including all the heat carriers loops of the different TES sections, with tanks, heat exchangers, pumps and air cooled heat rejection units. In particular the thermal energy storage is divided in five steps which differ in the adopted heat transfer fluid: TES0 allows to exploit the CO<sub>2</sub> heat of condensation released during charging mode for CO<sub>2</sub> evaporation during discharging mode, TES1-4 allows to exploits the sensible heat released from CO<sub>2</sub> cooling in charging mode to heat up CO<sub>2</sub> before expansion in discharging mode. The detailed description of TES assumptions is reported in section 3.3.

The merit index of the system is defined by the Round Trip Efficiency (RTE), calculated as the electrical energy produced in discharging mode divided by the energy consumed in charging mode. The RTE can be calculated accounting for (eq.1) or neglecting (eq.2) the consumption of the system auxiliaries, namely the pumps for the heat transfer fluid circulation and the fans for the heat rejection to the ambient with dry air coolers. Following sections give a description of main system components and the assumptions adopted in this study.

$$RTE_{net} = \frac{W_{turb} - \sum_{i=0}^4 W_{piD} - \sum_{i=0}^4 W_{pHRUi} - W_{PCHX}}{W_{comp} + \sum_{i=0}^4 W_{pic}} \quad (1)$$

$$RTE_{gross} = \frac{W_{turb}}{W_{comp}} \quad (2)$$

### 3.1 Boundary conditions

Table 1 resumes the main assumptions on system boundary conditions. Among them the most important one is the minimum temperature of cooling water used for the condensation of CO<sub>2</sub> in charging mode and for the CO<sub>2</sub> evaporation in discharging mode also determining the CO<sub>2</sub> pressure in the two operation modes. A value close to 22°C is assumed considering an approach point temperature difference equal to 7°C in the water/ambient air heat rejection unit.

**TABLE 1 – BOUNDARY CONDITION FOR NUMERICAL MODEL**

Ambient temperature, °C	15
T <sub>min</sub> cooling water (TES0), °C	21.9
Dome Temperature, °C	15
Dome pressure, bar	1.0085
Outlet pressure drop from dome	0.50%
Inlet pressure drop to dome	0.50%
CO <sub>2</sub> charging mass flow rate, kg/s	54
CO <sub>2</sub> discharging mass flow rate, kg/s	54

Moreover, we assumed to operate the system with the same CO<sub>2</sub> mass flow rate in both charging and discharging mode thus considering the same charging and discharging time. This allows having a similar size of compressor and turbine and a duty of each TES section similar in both operation modes.

### 3.2 Turbomachinery and Heat Rejection Unit

It is important to underline that the design of turbomachinery for this application is dramatically different from the design of turbine and compressor for supercritical CO<sub>2</sub> power cycles [24]. Main differences regards:

- the volumetric behavior of the fluid during compression which shows strong real gas effects in sCO<sub>2</sub> cycles while it is an ideal gas in this application;
- the minimum pressure which is typically 70-80 bar in sCO<sub>2</sub> cycles while it is equal to 1 bar for the present application;
- The pressure ratio which is 3-5 (leading to maximum pressures of 200-250 bar) in sCO<sub>2</sub> cycle and around 70 for CO<sub>2</sub> battery technology.

As a consequence the design of both turbine and compressor mainly refers to the best design practice for equipment working with air as those used for open gas cycles and CAES application.

Regarding the turbine, we carried out a preliminary design with the aim of maximizing the expansion efficiency and considering an overall volume ratio and isentropic enthalpy drop of 25 and 375 kJ/kg respectively.

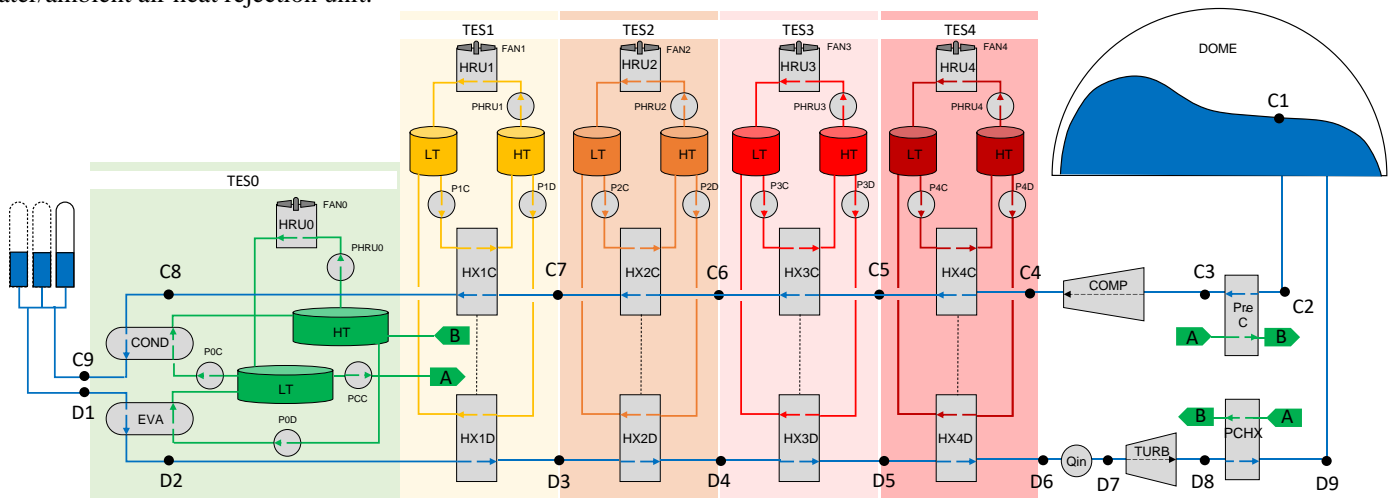


**FIGURE 2 - DETAILED SCHEME OF THE STORAGE SYSTEM AT THE BASIS OF THE NUMERICAL MODEL. THE USE OF PRECOOLER (C2-C3) AND OF THE ADDITIONAL HEATER (D6-D7) IS NOT ADOPTED IN THE PRESENT STUDY**

Mean diameter peripheral speed is selected equal to minimum CO<sub>2</sub> speed of sound (280 m/s at turbine exit), 50% reaction stages with loading coefficient ( $k_{is} = 2\Delta h/u_m^2$ ) equal to 2.5 are adopted and a maximum stage volume ratio is assumed equal to 3. Turbine suggested design has a mean diameter of 0.9 m, requires 4-6 axial stages and rotates at 6000 RPM. An alternative design at 3000RPM requires a larger number of stages (about 15/20) operating at low peripheral speed, with limited blade loading and at a favorable specific speed. If well designed, both turbines can reach an adiabatic efficiency consistent with the assumed value of 93%. Compressor design is based on the assumption of a different maximum stage volume ratio depending on the stage type: 1.25 for axial stages and 3 for radial ones. Regarding the compressor there are two possible designs: a multi stage radial compressor or a mixed axial-radial solution. The blade efficiency assumed in this study (85%) is consistent with the values achievable with the first solution. Higher efficiency values (in the range of 86-87%) could be obtained by adopting a mixed solution: a multistage axial flow compressor (14 stages), a solution usually adopted by gas turbine manufacturers for similar values of inlet flow rates and pressure ratios around 15, leaving the final compression to a single-stage transonic radial compressor.

Pumps efficiency have a limited effect on the overall plant performance but were included for a correct evaluation of RTE while electrical efficiency and mechanical efficiency for compressor and pump motor and generator refers to large scale components. Finally, heat rejection unit fan consumption is evaluated assuming a value of fan power with respect to released thermal power equal to 1%.

Table 2 reports the main assumptions related to turbomachinery and heat rejection unit auxiliary consumption.

### 3.3 Thermal heat storage (TES) configuration

A point which requires some additional explanation is the thermal energy storage (TES) system organization. Two different TES designs can be adopted for CO<sub>2</sub> battery technology: a dual media thermocline or a common system of two-tanks heat transfer fluid storage.

First option is made by an array of pressurized vessels filled by a high heat capacity (with respect to CO<sub>2</sub>) solid material: during charging mode CO<sub>2</sub> heats up the solid filler while the opposite in discharging mode.

The vessel number and arrangement (series and/or parallel) depends on the maximum vessel diameter (selected according to charging pressure), filler material properties (void fraction, heat capacity, particle sizes) and maximum allowable CO<sub>2</sub> pressure drops.

**TABLE 2 – ASSUMPTIONS ON TURBOMACHINERY EFFICIENCY**

$\eta_{compressor}$	85%	$\eta_{mechanic}$	99%
$\eta_{turbine}$	93%	$\eta_{electric}$	98.5%
$\eta_{pump}$	85%	$W_{fan}/Q_{HRU}$	1%

Different filler materials have been already tested at temperature higher than those required by CO<sub>2</sub> battery technology (around 450°C) on both static and cycling test carried out on both lab scale and relevant scale experimental campaigns [25, 26]. These activities demonstrated that quartzite and silica sand are appropriate filling materials for both molten salts and air applications [27]. The adoption of a dual media thermocline is attractive for a number of reasons related mainly to: (i) lower amount of metal mass, (ii) no issues related to pinch point temperature difference located within the heat exchangers, (iii) lower terminal temperature difference. However, dual media thermocline TES with high pressure CO<sub>2</sub> are not commercial components today and their development is a crucial step in the future assessment of EnergyDome SpA technology.

On the contrary, the second possible TES design is already available today from technological perspective as it refers to classic arrangement of thermal energy storage made by a two-tanks system and a countercurrent heat exchanger, a solution successfully adopted in a wide range of concentrated solar power (CSP) plants. During the charging phase the hot CO<sub>2</sub> stream cools down by transferring heat in the countercurrent heat exchanger to an energy carrier stream, which flows from the “cold” to the “hot” tank. During the discharging phase, the opposite path is followed: the heat carrier flows from the “hot” to the “cold” tank while heating up the CO<sub>2</sub> stream. However, the simple assumption of finite temperature differences at the heat exchanger terminals does not warrant that the process is feasible since the specific heat of both CO<sub>2</sub> and general heat carrier fluids experiences a different variation in the temperature range of interest. In particular, as reported in Figure 3, the specific heat of CO<sub>2</sub> is higher at low temperature due to real gas effects near the saturation dome, while specific heat of heat transfer fluids (HTF) increases with temperature.

As a consequence, if a single heat transfer fluid would be adopted, the pinch point, i.e. the minimum temperature difference between the two streams, will occur in an intermediate section of the heat exchanger, thus resulting into large temperature differences at the exchanger terminals to make the heat exchange possible.

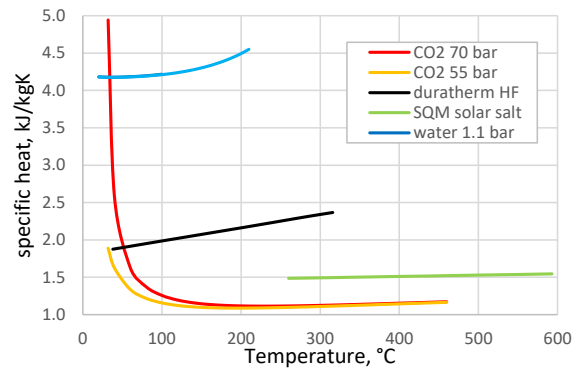


**FIGURE 3 - SPECIFIC HEAT VARIATION AS FUNCTION OF TEMPERATURE FOR CO<sub>2</sub> AT CHARGING AND DISCHARGING PRESSURE AND HTFs**

This fact would strongly penalize the system RTE leading to a lower temperature of the CO<sub>2</sub> at the turbine inlet and to a limitation of turbine specific work. The other difficulty is related to the availability of single HTF able to cover the temperature span from nearly ambient temperature to around 450°C without incurring in thermal degradation at high temperature or excessive viscosity increase/solidification at low temperature. To overcome these issues, it is necessary to divide the heat exchange in a few sections, selecting a proper heat capacity (the product of the mass flow rate and specific heat) of the heat carrier stream, in order to match the heat capacity of the CO<sub>2</sub> stream in each temperature span, following an approach similar to adiabatic CAES plants [9].

The Figure 2 depicts the proposed solution for CO<sub>2</sub> battery technology. The high temperature TES is divided in four steps TES1-TES4: in the first two (low temperature) the heat carrier is water at ambient pressure, with different flow rates; in the third and fourth the heat carriers are a Duratherm HF synthetic oil [28] and SQM solar salt [29] (binary mixture of KNO<sub>3</sub>/NaCl) respectively. The choice of the above heat carriers comes from the experience gained in CSP (Concentrating Solar Power) [30] plants and avoids operational problems keeping each HTF within its operative temperature range.

The design assumptions for each section of the overall TES system (TES0-TES4) are reported in Table 3 for the temperature differences and in Table 4 for the pressure drops. For high temperature TES heat exchangers a pinch point temperature difference equal to 7.5°C is assumed while for evaporator and condenser (TES0), we assumed values coming from the experience gained in the air conditioning and refrigeration, a sector where CO<sub>2</sub> is becoming more and more popular. Table 3 and Table 4 also report the main assumptions related to CO<sub>2</sub> post cooler heat exchanger after the expansion and the heat rejection units. It is important to underline that assumptions on minimum cooling water temperature and temperature difference in condenser and evaporator also determine the CO<sub>2</sub> charging and discharging pressures which are not subject to optimization. However, the impact of these assumptions on calculated RTE is investigated by means of a sensitivity analysis at the end of this paper.

#### 3.4 Thermal losses

We assume that the heat storage tanks will be well insulated. However, some thermal losses will be unavoidable. We assume that 1% of the heat stored during the charging phase will be lost in the time interval between the charging and the discharging phase. This means, in example, that the “hot” tanks during the discharging phase will be at a temperature lower than the one reached in the charging phase.

#### 4. OPTIMIZATION PROCEDURE

Each simulated case is optimized with the aim of maximizing the net round trip efficiency (RTE) by varying the following quantities:

- Switch temperatures of CO<sub>2</sub>: namely the temperatures of CO<sub>2</sub> outlet from each thermal storage heat exchanger

during the charging phase (C5, C6, C7 and C8). These parameters: (i) define the heat repartition within the four thermal energy storage systems, (ii) influence the maximum temperature reached by the various heat carrier fluids due to pinch-point temperature difference limitation, (iii) define the heat transfer area required for each thermal storage section.

- hot side temperature difference of each thermal storage heat exchanger in the discharging phase. These parameters: (i) influences the heat exploited during discharge, (ii) the heat transfer area and (iii) the maximum temperature reached by the CO<sub>2</sub>

The temperature in C8 also determines the degree of superheating with respect to condensation temperature in charging mode while hot side temperature difference for the evaporator determines the degree of superheating in the evaporator.

**TABLE 3 – ASSUMPTIONS ON HEAT EXCHANGER TEMPERATURE DIFFERENCE**

<b>TES0 -Condenser (charging)</b>	
$\Delta T_{pp}$ charging, °C	2.0
$\Delta T$ (CO <sub>2</sub> cond - Tmin cooling water), °C	3.6
$\Delta T$ (CO <sub>2</sub> subcooled-Tmin cooling water), °C	2.6
<b>TES0 - Evaporator (discharging)</b>	
$\Delta T$ (Tmin cooling water - CO <sub>2</sub> eva), °C	2.00
<b>Post cooler (discharging)</b>	
$\Delta T_{pp}$ , °C	5.00
<b>Heat rejection units</b>	
Minimum $\Delta T_{pp}$ (real $\Delta T$ can be larger), °C	7
<b>Thermal energy storage (charging)</b>	
HTF fluid	TES1    TES2    TES3    TES4
	H2O    H2O    T.Oil    M.Salt
$\Delta T_{pp}$ charging, °C	7.5    7.5    7.5    7.5

**TABLE 4 – ASSUMPTIONS ON HEAT EXCHANGER PRESSURE DROPS**

<b>TES0 - Condenser (charging)</b>	
$\Delta T$ condenser ( $\Delta p$ cond), °C	0.5
$\Delta p$ SH	0%
$\Delta p$ SC, bar	0
$\Delta p$ water, bar	0.5
<b>TES0 - Evaporator (discharging)</b>	
$\Delta T$ evaporator ( $\Delta p$ eva), °C	0.5
$\Delta p$ SH	0%
$\Delta p$ water, bar	0.5
<b>Post cooler (discharging)</b>	
$\Delta p$ CO <sub>2</sub> post cooler	0.5%
<b>Heat rejection units</b>	
$\Delta p$ HTF in HRU, bar	0.5
<b>TES1-TES4 (charging and discharging)</b>	
$\Delta p$ CO <sub>2</sub> TES1-4 (overall), bar	4.00%
$\Delta p$ for each HTF, bar	1

Optimization parameters are varied respecting the following constraints:

- For each thermal storage section, the heat carrier fluid mass flow rate in discharging phase must be  $\leq$  than the same quantity in charging phase. If lower an additional consumption related to the fans of heat rejection unit is introduced in order to restore the initial condition of energy storage at the end of the discharging phase.
- The possibility to use the same heat exchanger for charging and discharging operation is introduced in an approximate way. The heat transfer area required in discharging phase is constrained to be  $\leq$  than the area in charging phase. Considering constant heat transfer coefficients in both phases, this constraint implies that, during real discharge operation, the heat exchangers will be oversized and will operate with a higher effectiveness with positive effects on system efficiency. The results obtained with this constraint are thus conservative and avoid excessive size of the heat exchangers at the same time.
- Heat carrier fluid temperature must be always within the fluid operative temperature range as defined by the manufacturer datasheet
- No temperature difference is allowed between maximum storage temperature of a TES and minimum storage temperature of the following TES resulting in a continuous T-Q profile of the HTFs. This additional constraint may lead to suboptimal solutions but it has been verified that its effect on the RTE is limited when adopting a large number of different TES section as in this case.

As result the maximum temperature of each HTFs is defined during charging mode calculation leading to the calculation of CO<sub>2</sub> temperatures in discharging mode.

## 5. RESULTS ON SYSTEM PERFORMANCE

Results are presented in two sections: first section presents the detailed results for the reference case configuration with a full description of all the streams thermodynamic properties while the second one shows the results of a sensitivity analysis applying changes to some of the assumptions of the reference case.

### 5.1 Detailed results

In the detailed calculation the actual consumption of all the system auxiliaries is included into the analysis and the TES arrangement is optimized in order to maximize net RTE. Optimal values of design parameters for the four CO<sub>2</sub> temperature switch (namely the CO<sub>2</sub> outlet temperature from TES in charging mode) and the five discharging terminal hot end temperature differences for TES0-4 are reported in Table 5.

**TABLE 5. – OPTIMAL DESIGN PARAMETERS VALUES**

TES	0	1	2	3	4
$T_{switch}$ , °C, $\Delta\text{Thot end}$ , °C	4.05	7.04	2.75	5.13	6.44

Figure 4 depicts the Temperature-specific entropy diagram of the optimized process where it is possible to appreciate the difference in pressure between charging and discharging mode and the role of the post cooler heat exchanger after the expansion. Table 6 describes the power balance the two phases. The net round trip efficiency is equal to 76.9%.

Optimization procedure pushes the system towards a solution which minimizes the heat dissipation in TES1-4. In particular, it is possible to highlight that the heat stored in the hot storage system (TES1-TES4) during charging phase is totally exploited during discharge while a small heat excess (472.8 kW, 5.72%) is present only at the TES0 (condenser-evaporator). In order to guarantee the initial storages state of charge at the end of the charging-discharging cycle, this heat excess must be rejected (as well as the heat associated to CO<sub>2</sub> post cooling) to the ambient through a heat rejection unit causing additional pump and fan consumption.

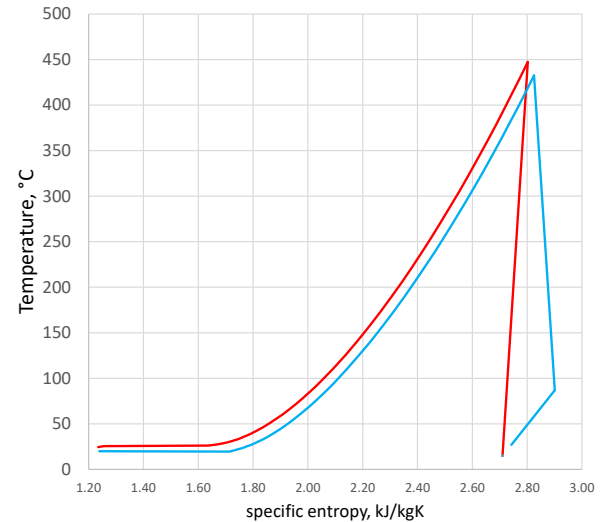


**FIGURE 4 – T-s DIAGRAM FOR THE CHARGING (RED) AND DISCHARGING (BLUE) PHASES**

**TABLE 6 - POWER BALANCE (kW) OF THE COMPUTED REFERENCE CASE**

Power balance	Charging	Discharging
$W_{comp}$ or $W_{turb}$	23633	18362
$W_{pump}$ TES0	44.53	41.95
$W_{pump}$ PCHX	-	15.50
$W_{pump}$ TES1	3.26	3.26
$W_{pump}$ TES2	4.68	4.68
$W_{pump}$ TES3	12.03	12.03
$W_{pump}$ TES4	10.16	10.17
$W_{pump}$ HRU TES0	-	18.08
$W_{fan}$ TES0	-	33.18
$W_{net}$	23708	18224
$RTE_{gross}$		77.7%
$RTE_{net}$		76.9%

Tables 7-8 report the thermodynamic conditions of CO<sub>2</sub> in the two phases and the TES operating conditions.

Figure 5 depicts the temperature-heat and the temperature difference-heat diagrams for the charging and discharging phase. It is possible to highlight that the choice of adopting four levels of TES for storing the sensible heat of CO<sub>2</sub> allows to always have a good match between CO<sub>2</sub> and HTF with limited temperature differences also within the heat exchangers. Final positive result is to reach a turbine inlet temperature which is very close to the compressor outlet temperature thus maximizing discharge power output.

**TABLE 7 - CO<sub>2</sub> THERMODYNAMIC PROPERTIES,**  
G-gaseous stream, sV-saturated vapor, sL-saturated liquid, scL-  
subcooled liquid, mix-two phase flow

Charging						
	T, °C	p, bar	h, kJ/kg	s, kJ/kgK	ρ, kg/m <sup>3</sup>	state
C1	15.00	1.01	497.39	2.71	1.86	G
C2	14.99	1.00	497.39	2.71	1.85	G
C3	14.99	1.00	497.39	2.71	1.85	G
C4is	392.21	68.58	860.15	2.71	54.77	G
C4	447.42	68.58	924.16	2.80	50.27	G
C5	269.30	67.88	721.17	2.48	68.25	G
C6	110.83	67.19	542.64	2.09	108.39	G
C7	50.18	66.51	459.68	1.86	157.96	G
C8	33.18	65.84	423.85	1.75	197.53	G
C8V	26.00	65.84	390.71	1.64	255.86	sv
C8L	25.50	65.09	276.98	1.26	702.70	sL
C9	24.50	65.09	270.92	1.24	727.62	scL
Discharging						
	T, °C	p, bar	h, kJ/kg	s, kJ/kgK	ρ, kg/m <sup>3</sup>	state
D1	19.90	57.16	270.92	1.24	594.36	mix
D1V	19.40	56.49	409.10	1.71	189.61	sV
D2	20.52	56.49	413.57	1.73	183.08	G
D3	34.62	55.91	449.03	1.85	141.24	G
D4	94.26	55.35	531.17	2.09	93.02	G
D5	254.11	54.79	707.92	2.50	56.62	G
D6	432.59	54.23	908.88	2.83	40.67	G
D7	432.59	54.23	908.88	2.83	40.67	G
D8is	57.42	1.02	533.92	2.83	1.64	G
D8	86.75	1.02	560.17	2.90	1.50	G
D9	26.90	1.01	507.46	2.74	1.80	G

**TABLE 8 - HEAT CARRIER FLUIDS INLET AND OUTLET CONDITIONS FROM ALL THE TES SUBSYSTEMS**

	T <sub>min</sub> , °C	T <sub>max</sub> , °C	m, kg/s	Q, kW
TES0 C	21.90	24.58	736.50	8259
TES0 D	21.91	24.57	693.90	7703
TES1 C	24.58	41.75	26.96	1934
TES1 D	24.67	41.66	26.96	1915
TES2 C	41.75	97.29	19.24	4480
TES2 D	42.03	97.02	19.24	4435
TES3 C	97.29	260.00	27.89	9641
TES3 D	98.16	259.24	27.89	9544
TES4 C	260.00	439.92	40.53	10961
TES4 D	260.91	439.03	40.53	10852

## 5.2 Sensitivity analysis

We believe that the assumptions made for computing the plant performance are representative of the current state-of-the-art for equipment design. However, we carried out also a sensitivity analysis to verify the effect of possible deviations on some of the assumptions. We based the sensitivity analysis according to Table 9 which reports the variability range for the design parameters which have the largest impact on system RTE: turbine and compressor efficiency, heat exchangers temperature differences, pressure drops and thermal losses.

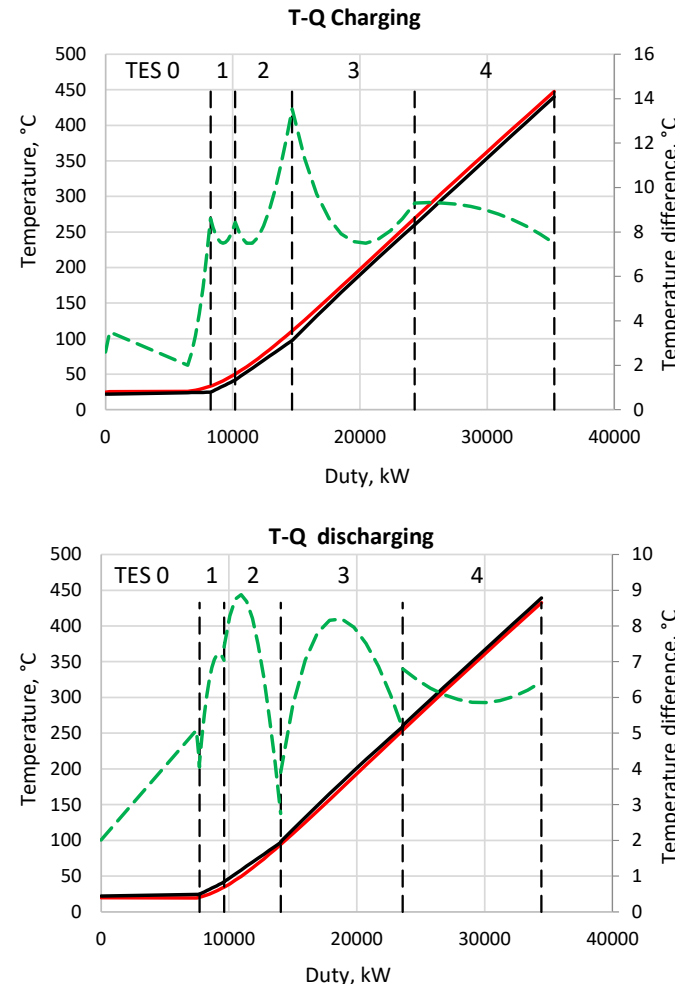


**FIGURE 5 –PROFILES FOR CO<sub>2</sub> (RED), HTF (BLACK), TEMPERATURE DIFFERENCE (GREEN) IN THE CHARGING AND DISCHARGING PHASES**

**TABLE 9. - SENSITIVITY ANALYSIS ASSUMPTIONS**

Parameter	ref	Worst case	Best case
Turbine efficiency	0.93	0.91 (-2%)	0.95(+2%)
Compressor efficiency	0.85	0.83 (-2%)	0.87(+2%)
TES 1-4 charging ΔT <sub>pp</sub>	7.5	10 (+33%)	5 (-33%)
Condenser-evaporator ΔT	Table 3	ref +50%	ref -50%
Pressure drops CO <sub>2</sub> and HTF	Table 4	ref +50%	ref -50%
Thermal losses	1%	2%	0%

Figure 6 summarizes the results of this analysis. The figure demonstrates that even significant variations on the assumptions made do not cause large deviations from the outstanding value of the round trip efficiency obtained by the present analysis. The turbine efficiency plays the most significant role but it is the authors' opinion that the stipulated value (93%) is fully consistent with the state of the art of fluid-dynamic design. The figure outlines also the importance of the heat transfer equipment, both in terms of thermal performance and pressure loss.

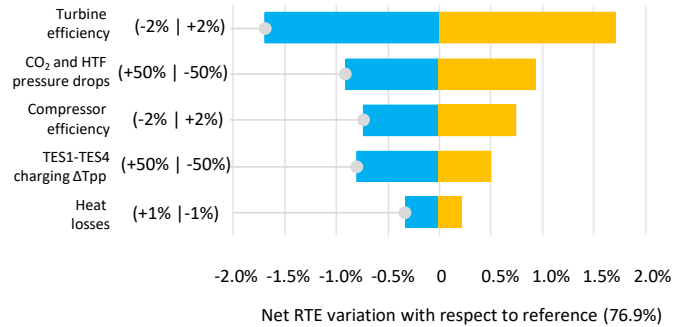


**FIGURE 6 TORNADO CHART OF SENSITIVITY ANALYSIS ON THE NET RTE OF DETAILED SIMULATION**

## 6. COMPONENTS SIZING AND COST ESTIMATION

While the prediction of the system footprint (FP) is a simple, straightforward procedure, the accurate estimation of the system cost would require a detailed design of all components as well as the acquisition of offers from manufacturers. This procedure is beyond the scope of the present paper, however, we performed a rough estimation of costs, mostly based on literature correlations, precise enough to confirm the economic viability of the proposed system. Calculation of system footprint and cost is carried out for a system with 5 equivalent hours of storage capacity and 250 cycles a year. The pre-sizing of the equipment and the system footprint is estimated knowing the thermodynamic properties of the streams and introducing the following assumptions:

- Ambient pressure storage is designed as a single semispherical dome while the liquid CO<sub>2</sub> storage is designed as a set of 55 vertical tanks with diameter of 2 m and 8 m tall;
- Each energy storage TES1-2-3-4 (CO<sub>2</sub> sensible heat) encompasses two low pressure tanks with height to diameter ratio equal to one and diameters between 7 and 8 meters. TES0 (CO<sub>2</sub> latent heat) is designed as a 1325m<sup>2</sup> water pit with depth of 10 meters;
- Heat transfer area of heat exchangers is evaluated considering a global heat transfer coefficient of 800 W/m<sup>2</sup>K for gaseous CO<sub>2</sub> equipment (HX1-2-3-4) and 3000 W/m<sup>2</sup>K for CO<sub>2</sub> in phase transition heat exchangers (COND/EVA). A surface to volume ratio equal to 100 m<sup>2</sup>/m<sup>3</sup> [31] and a length to diameter ratio equal to 5 are assumed;
- Turbomachinery island is assumed equal to 300 m<sup>2</sup>.

- For overall footprint calculation equipment footprint is increased by 50%

Table 10 summarizes main component dimensions and overall system footprint while a possible system layout is also reported in figure 7. The system footprint is around 11% of the extension of a photovoltaic panels field able to provide the compressor nominal power (189000 m<sup>2</sup>) calculated considering a land to panel surface ratio equal to 2, a global irradiance of 1000 W/m<sup>2</sup> and conversion efficiency of 25%.

**TABLE 10. – EQUIPMENT PRE-SIZING AND FOOTPRINT**

Heat Exch.	Area, m <sup>2</sup>	D., m	L., m	units	FP, m <sup>2</sup>	%
COND/EVA	1375	1.4	7.0	1	9.8	0.05%
HX1	431	1.0	4.8	1	4.5	0.02%
HX2	848	1.2	6.0	1	7.1	0.03%
HX3	1979	1.6	7.9	1	12.5	0.06%
HX 4	2218	1.6	8.2	1	13.5	0.06%
Heat exchangers total, m <sup>2</sup>					47.4	0.22%
TES Tanks	Vol., m <sup>3</sup>	D., m	H., m	units	FP, m <sup>2</sup>	%
TES0	13257.6		10	1	1325.8	6.18%
TES1	485.3	8.5	8.5	2	57	0.27%
TES2	346.3	7.6	7.6	2	45.5	0.21%
TES3	278.9	7.1	7.1	2	39.4	0.18%
TES4	429.2	8.2	8.2	2	52.5	0.24%
TES Tanks total, m <sup>2</sup>					1520.2	7.08%
CO <sub>2</sub> storage	Vol., m <sup>3</sup>	D., m	H., m	units	FP, m <sup>2</sup>	%
Liquid	1335.9	2	8	55	173	0.80%
Gaseous	521732.2	125	62.5	1	12266	57.2%
CO <sub>2</sub> storage total, m <sup>2</sup>					12438	58%
Turbomachinery island, m <sup>2</sup>					300	1.40%
Additional land occupation, m <sup>2</sup>					7153	33.3%
<b>Overall Footprint, m<sup>2</sup></b>					<b>21459</b>	<b>100%</b>

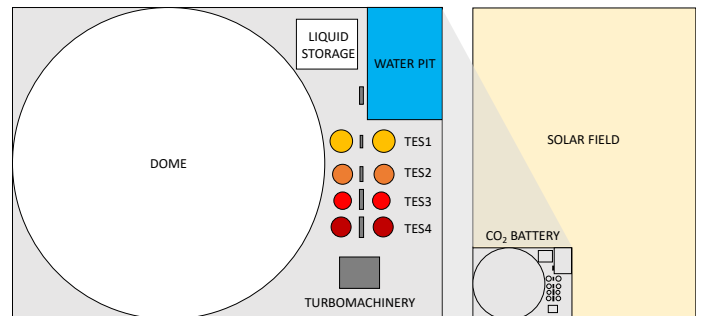


**FIGURE 7 SYSTEM LAYOUT AND COMPARISON WITH SOLAR FIELD AREA TO POWER THE PROPOSED SYSTEM**

System cost can be evaluated using equipment cost functions from literature.

- Dome specific cost is assumed equal to 7.2 \$/m<sup>3</sup> while cost of liquid storage is evaluated with cost correlation for vertical vessels [32];
- Storage tank cost is calculated with carbon steel cone roof tank cost correlation [32] increased by a factor of 2 in order to account for heavy insulation while water pit storage specific cost is assumed equal to 36 \$/m<sup>3</sup> [33];
- Heat transfer fluid cost is assumed equal to 1 \$/m<sup>3</sup> for water, 2 \$/kg for thermal oil and 1.25\$/kg for molten salt.
- Capital cost of heat exchangers is evaluated with cost correlation for Shell and Tubes heat exchangers [32];
- Turbomachinery cost correlation is not available in literature considering the very specific application. However, the dimensions and the number of stages of the CO<sub>2</sub> compressor and turbine are not too dissimilar to the LM2500 GE turbine which features a 16 stages axial compressor and a 2HP+6LP axial stages turbine. LM2500 cost is around 12M\$ (generator included) [34] while for CO<sub>2</sub> battery turbomachinery a value of 8M\$ can be reasonably assumed considering the absence of blade cooling, double speed shaft, combustor and accounting for the lower temperature which does not require superalloys.
- Land cost, Balance of Plant and instrumentation are assumed equal to 30% of the sum of equipment capital cost [35]

Table 11 summarizes the breakdown of system capital cost calculated with cost correlations while Table 12 reports the Levelized Cost of Storage (LCOS). LCOS is calculated by assuming first year Carrying Charge Fraction (CCF) equal to 0.1 and fixed and variable O&M suggested for CAES technology and equal to 7 \$/kW-year and 0.3 cents/kWh respectively [36]. LCOS results equal around 115\$/MWh which makes this technology competitive against underground and above ground CAES which LCOS is around 100€/MWh (120\$/MWh) and electrochemical batteries having LCOS from 200 and 400 €/MWh depending on the technology [37].

**TABLE 11. – EQUIPMENT AND SYSTEM CAPITAL COST**

<b>TES, k\$</b>	<b>HX</b>	<b>Tank/pit</b>	<b>HTF</b>	<b>%</b>
TES0	150	479	13	2.7%
TES1	45	360	0.5	1.7%
TES2	83	330	0.3	1.7%
TES3	225	300	1004	6.5%
TES4	255	360	897	6.4%
<b>TES total cost, k\$</b>		<b>4502</b>		<b>19.0%</b>
Turbomachinery		8000		33.8%
Dome storage, k\$		3771.6		15.9%
CO <sub>2</sub> liquid storage, k\$		2393.1		10.1%
Balance of Plant, k\$		5025.4		21.2%
<b>Total cost, M\$</b>		<b>23.7</b>		<b>100%</b>

**TABLE 12. – LCOS ASSUMPTIONS AND CALCULATION**

first year Carrying Charge Fraction	0.1	
Fixed O&M, \$/kW-year	7	
Variable O&M, \$cents/kWh	0.3	
Number of cycles a year and duration	250-5h	
Annual Energy in discharge, MWh	22953	
	annual cost, M\$	LCOS, \$/MWh
Capital cost fraction	2.37	103.22
fixed O&M	0.165	7.21
variable O&M	0.069	3.00
<b>Total</b>	<b>2.60</b>	<b>113.43</b>

## 7. CONCLUSIONS

The CO<sub>2</sub> battery system exhibits a number of relevant advantages over the other storage systems proposed in the scientific literature and implemented in prototypes or relevant scale applications:

- It is not site dependent: can be located in any site, since it doesn't require the existence of underground caverns, nor favorable orographic conditions;
- With the exception of turbomachinery, its components are all already available on the market, resulting in a technology that can easily exploit technologic transfer from other industrial fields;
- According to our calculations, its performance can reach a realistic net roundtrip efficiency higher than 75%, thus better than most other storage systems;
- System cost calculated with correlation from reference confirm the economic viability of the proposed system in comparison to other competitive solutions assessing a final LCOS of around 115\$/MWh;
- It ensures long lifetime of the components (>25 years) and limited performance decay as any mechanical system.
- It adopts a maximum pressure which is lower than CAES, LAES, and other proposed storage systems using CO<sub>2</sub> as working medium thus allowing for more compact and economic turbomachinery;
- It works between a constant minimum pressure (ambient) and a constant maximum pressure (condensation) at all times differently from CAES systems. This leads to turbomachinery with constant pressure ratio during charging and discharging modes always characterized by high efficiency;
- It adopts thermal energy storage solutions that are already available on the market for industrial application and CSP power plants;
- It has great flexibility, being able to pass from energy storage to full power output and vice versa in a matter of seconds. It can operate from zero to at nominal power both in the charge and discharge phases;
- It has no limit of depth of discharge and storage can be deployed completely without any loss of performance;
- The calculations performed in this paper refer to a storage system of about 100 MWh with nominal power of about 20 MW. However, the system inherent modularity can cover a wide range of energy storage and power.

## REFERENCES

- [1] IRENA, International Renewable Energy Agency, *Renewable Power Generation Costs in 2019, 2020*.
- [2] BritishPetroleum, *Statistical Review of World Energy 2020. 69th edition*, 2020.
- [3] IEA-ET SAP e IRENA, *Technology Brief E15 – Renewable Energy Integration in Power Grids*, 2015.
- [4] E. Redondo-Iglesias, P. Venet e S. Pelissier, «Efficiency Degradation Model of Lithium-ion Batteries for Electric Vehicles,» *IEEE Transactions on Industry Applications*, vol. 55, n. 2, pp. 1932 - 1940, 2019.
- [5] M. Schimpe, M. Naumann, N. Truong, H. C. Hesse, S. Santhanagopalan, A. Saxon e A. Jossen, «Energy efficiency evaluation of a stationary lithium-ion battery container storage system via electro-thermal modeling and detailed component analysis,» *Applied Energy*, vol. 210, pp. 211-229, 2018.
- [6] K. Smith, A. S. M. Keyser, B. Lundstrom, Z. Cao e A. Roc, «Life Prediction Model for Grid-Connected Li-ion Battery Energy Storage System,» in *American Control Conference*, Seattle, Washington, 2017.
- [7] R. H. W. Samir Succar, *Compressed Air Energy Storage: Theory, Resources, And Applications For Wind Power*, Princeton Environmental Institute, 2008.
- [8] S. K. K. Mandhapati Raju, «Modeling and simulation of compressed air storage in caverns: A case study of the Huntorf plant,» *Applied Energy*, vol. 89, n. 1, pp. 474-481, 2012.
- [9] M. Astolfi, G. Guandalini, M. Belloli, A. Hirn, P. Silva e S. Campanari, «Preliminary Design and Performance Assessment of an Underwater Compressed Air Energy Storage System for Wind Power Balancing,» *ASME. J. Eng. Gas Turbines Power*, 2020.
- [10] F. Crotogino, K.-U. Mohmeyer e R. Scharf, *Huntorf CAES: More than 20 Years of Successful Operation*, 2001.
- [11] ESA Energy Storage Association, «Compressed Air Energy Storage (CAES),» [Online]. Available: <https://energystorage.org/why-energy-storage/technologies/compressed-air-energy-storage-caes/>. [Consultato il giorno 22 11 2020].
- [12] G. L. Guizzi, M. Manno, L. M. Tolomei e R. M. Vitali, «Thermodynamic analysis of a liquid air energy storage system,» *Energy*, vol. 93, n. 2, pp. 1639-1647, 2015.
- [13] Highview Power, «Cryogenic energy storage,» [Online]. Available: <https://highviewpower.com/technology/>. [Consultato il giorno 22 11 2020].
- [14] ESA - Energy Storage Association, «Hydrogen Energy Storage,» [Online]. Available: <https://energystorage.org/why-energy-storage/technologies/hydrogen-energy-storage/>.
- [15] J. D. McTigue, A. J. White e C. N. Markides, «Parametric studies and optimisation of pumped thermal electricity storage,» *Applied Energy*, vol. 137, pp. 800-811, 2015.
- [16] B. Eppinger, L. Zigan, J. Karl e S. Will, «Pumped thermal energy storage with heat pump-ORC-systems: Comparison of latent and sensible thermal storages for various fluids,» *Applied Energy*, vol. 280, 2020.
- [17] A. Smallbone, V. Jülich, R. Wardle e A. P. Roskilly, «Levelised Cost of Storage for Pumped Heat Energy Storage in comparison with other energy storage technologies,» *Energy Conversion and Management*, vol. 152, pp. 221-228, 2017.
- [18] MALTA inc., «Malta's Electro-Thermal Energy Storage System,» [Online]. Available: <https://www.maltainc.com/>.
- [19] H. Liu, Q. He, A. Borgia, L. Pan e C. M. Oldenburg, «Thermodynamic analysis of a compressed carbon dioxide energy storage system using two saline aquifers at different depths as storage reservoirs,» *Energy Conversion and Management*, vol. 127, pp. 149-159.
- [20] F. Ayachi, N. Tauveron, T. Tariére, S. Collasson e D. Nguyen, «Thermo-Electric Energy Storage involving CO<sub>2</sub> transcritical cycles and ground heat storage,» *Applied Thermal Engineering*, vol. 108, pp. 1418-1428, 2016.
- [21] J. McTigue, P. Farres-Antunez, K. Ellingwood, T. Neises e A. White, *Pumped Thermal Electricity Storage with Supercritical CO<sub>2</sub> Cycles and Solar Heat Input*, NREL, 2019.
- [22] Energy Dome, «Groundbreaking Long Duration Energy Storage,» [Online]. Available: <https://energycdome.it/>.
- [23] E. Lemmon, I. Bell, M. Huber e M. McLinden, *NIST Standard Reference Database 23: Reference Fluid Thermodynamic and Transport Properties-REFPROP, Standard Reference Data Program*, Gaithersburg: National Institute of Standards and Technology, 2018.
- [24] D. Alfani, M. Astolfi, M. Binotti e P. Silva, «Part Load Strategy Definition and Annual Simulation for Small Size sCO<sub>2</sub> Based Pulverized Coal Power Plant,» in *Proceedings of the ASME Turbo Expo 2020: Turbomachinery Technical Conference and Exposition*, 2020.
- [25] D. A. Brosseau, P. F. Hlava e M. J. Kelly, *Testing Thermocline Filler Materials and Molten-Salt Heat Transfer Fluids for Thermal Energy Storage Systems Used in Parabolic Trough Solar Power Plants*, SANDIA, 2014.
- [26] J.-F. Hoffmann, T. Fasquelle, V. Goetz e X. Py, «A thermocline thermal energy storage system with filler materials for concentrated solar power plants: Experimental data and numerical model sensitivity to different experimental tank scales,» *Applied Thermal Engineering*, vol. 100, pp. 753-761, 2016.
- [27] Y. Jemmal, N. Zari e M. Maaroufi, «Experimental characterization of siliceous rocks to be used as filler

- materials for air-rock packed beds thermal energy storage systems in concentrated solar power plants,» *Solar Energy Materials and Solar Cells*, vol. 171, pp. 33-42, 2017.
- [28] Duratherm, «Duratherm HF - Technical data sheet,» [Online]. Available: <https://durathermfluids.com/it/products/duratherm-hf/>.
  - [29] SQM, «Thermo-solar Salts,» [Online]. Available: <https://www.sqm.com/wp-content/uploads/2018/05/Solar-salts-Book-eng.pdf>.
  - [30] M. Binotti, M. Astolfi, S. Campanari, G. Manzolini e P. Silva, «Preliminary assessment of sCO<sub>2</sub> cycles for power generation in CSP solar tower plants,» *Applied Energy*, vol. 204, pp. 1007-1017, 2017.
  - [31] D. Reay, C. Ramshaw e A. Harvey, «Chapter 4 - Compact and micro-heat exchangers,» in *Process Intensification, Engineering for Efficiency, Sustainability and Flexibility*, 2008, pp. 77-101.
  - [32] H. Loh, J. Lyons e C. W. White, «Process Equipment Cost Estimation,» DOE/NETL, January 2002.
  - [33] solarthermalworld, «Seasonal pit heat storage: Cost benchmark of 30 EUR/m<sup>3</sup>,» [Online]. Available: <https://www.solarthermalworld.org/news/seasonal-pit-heat-storage-cost-benchmark-30-eurm3>.
  - [34] Forecast International, «The Market for Gas Turbine Marine Engines 2010-2019,» 2010.
  - [35] B. McGrail, J. Cabe, C. Davidson, F. Knudsen, D. Bacon, M. Bearden, M. Chamness, J. Horner, S. Reidel, H. Schaeff, F. Spane e P. Thorne, «Techno-economic Performance Evaluation of Compressed Air Energy Storage in the Pacific Northwest,» 2013.
  - [36] V. Viswanathan, M. Kintner-Meyer, P. Balducci e C. Jin, «National Assessment of Energy Storage for Grid Balancing and Arbitrage PhaseII, Volume 2: Cost and Performance Characterization,» DOE, Pacific Northwest National Laboratory.
  - [37] B. Zakeri e S. Syri, «Electrical energy storage systems: A comparative life cycle cost analysis,» *Renewable and Sustainable Energy Reviews*, vol. 42, pp. 569-596, 2015.